IEEE Access
Multidisciplinary | Rapid Review | Open Access Journal

Received April 22, 2019, accepted June 5, 2019, date of publication June 19, 2019, date of current version July 23, 2019.

Digital Object Identifier 10.1109/ACCESS.2019.2923794

A Hierarchical Self-Regulation Control for Economic Operation of AC/DC Hybrid Microgrid With Hydrogen Energy Storage System

HANQING YANG[1], (Student Member, IEEE), QI LI[1], (Senior Member, IEEE), SHUDAN ZHAO[1], WEIRONG CHEN[1], (Senior Member, IEEE), AND HONG LIU[2,3]

[1]School of Electrical Engineering, Southwest Jiaotong University, Chengdu 611756, China
[2]Energy Research Institute, National Development and Reform Commission, Beijing 100824, China
[3]Academy of Macroeconomic Research, National Development and Reform Commission, Beijing 100824, China

Corresponding author: Qi Li (liqi0800@163.com)

This work was supported in part by the Application Foundation Project of Science and Technology Plan of Sichuan Province under Grant 19YYJC0698, and in part by the National Key Research and Development Program of China under Grant 2017YFB1201003.

ABSTRACT The introduction of hydrogen energy storage system (HESS) as a potential form of energy storage systems (ESSs) has a significant impact on original control and operation. This paper presents a hierarchical self-regulation control method, which can be divided into the supervisory layer and local layer control. The supervisory layer control decides the output power of ESSs, according to the operation cost function so that the system can reach economic optimum during the operation process. The local layer control adopts virtual inertia control with global power support to improve system stability. First, a HESS model composed of an electrolyzer, hydrogen storage tank, and the fuel cell is established. SOCH of hydrogen tank is defined to express produced and consumed hydrogen. Then, aiming at supervisory layer control, operation cost functions of battery energy storage system (BESS) and HESS under different operation modes are built. Virtual inertia of ac ESS and virtual capacitance of dc ESS are introduced for local layer control. Finally, the simulation results based on the RT-LAB platform of both 24-h operation case and step power change case verify the correctness of the proposed method. The comparison with only droop control method shows that the proposed method can achieve the lowest operation cost and improve system inertia.

INDEX TERMS AC/DC microgrid, hydrogen energy storage system (HESS), hierarchical control.

I. INTRODUCTION

Renewable energy generation has become a promising power generation means, due to the declining reserves of traditional fossil energy [1], [2]. Among them, photovoltaic (PV) power generation and wind power generation are widely used all over the world for its advantages of convenience, freely use, and environmentally friendly. However, renewable energy generation has inherent characteristics of uncertainty and intermittence, which remains obstacles of its application [3]–[5]. AC/DC hybrid microgrid is an effective solution to supply different AC and DC loads, and simultaneously to integrate with renewable energy sources (RESs) efficiently and reliably [6]–[8].

The associate editor coordinating the review of this manuscript and approving it for publication was Alexander Micallef.

The AC/DC hybrid microgrid attracts increasingly attention for high system efficiency and flexible operation modes in recent years. In AC/DC hybrid microgrid, AC subgrid can provide connection between utility grid and microgrid, which enable system operate both in grid-connected mode and islanded mode. Furthermore, power loss on converters can be reduced, as DC loads can be fed directly in DC subgrid.

In order to balance power fluctuation and realize autonomous operation, energy storage systems (ESSs) are usually introduced to AC/DC hybrid microgrid as energy buffer area [9]–[11]. In grid-connected operation mode, if power produced by all distributed sources (DSs) including ESSs, cannot satisfy load demand, insufficient power is provided by utility grid. Otherwise, surplus power is injected into utility grid. Thus, the impact of ESS on power balance is

not emphasized in this operation mode, due to power support of utility grid. On the contrary, in the islanded operation mode, ESS will play a significant role in power balance and voltage/frequency regulation [12]–[14]. Based on this situation, this paper mainly focuses on the control of AC/DC hybrid microgrid with multi-energy storage systems (MESSs) operating in the islanded mode.

On the technologies level, ESSs can be classified into mechanical storage, electrical storage, thermal storage, chemical storage and electrochemical storage [15]–[17]. When selecting a suitable ESS, operation cost, efficiency, service life and power respond time should be taken into consideration. For example, battery energy storage systems (BESSs) own high efficiency, but have the disadvantage of high energy consumption. Pumped hydroelectric systems can be applied in a large-scale situation, however there are some special requirements of installation sites [18].

Hydrogen energy is generally recognized as the most promising secondary energy in twenty-first Century. It has the characteristics of clean, free pollution, convenient storage and transportation, and high utilization rate which has attracted worldwide attention [19], [20]. A hydrogen energy storage system (HESS) is defined as a chemical storage technology due to the conversion between chemical energy and electrical energy. In contrast to BESS, this power conversion process is implemented together with fuel cell, electrolyzer, and hydrogen tank, which can be applied in both energy and power occasion.

At present, hydrogen energy technologies have been studied in many aspects, especially power application. In [18] and [21], an energy management strategy is proposed for an isolated microgrid with a hydrogen production and storage system. Reference [22] introduces the applications of HESS in wind power generation. Reference [23] presents the application of hydrogen energy in tramway through fuel cells, which can effectively improve system flexibility and reduce environment pollution. It can be seen from the above studies that hydrogen energy system may lead to greater flexibility of load demanding and can ensure both long and short-term energy storage, which also brings new challenges to microgrid control at the same time.

In traditional AC/DC hybrid microgrid, droop control which possess the advantages of high stability and flexibility without communication network is usually used to realize power distribution between DGs in both AC and DC subgrids [24], [25]. However, droop control also requires coordination between power allocation accuracy and voltage deviation. In order to overcome these problems, the improved droop control is proposed [23], [26], [27]. In order to achieve the maximum utilization rate of renewable energy, RESs usually adopt maximum power tracking control method. That makes the control of ESS in AC/DC hybrid microgrid become particularly important. In [24], a distributed control strategy of energy storage unit applied in a three-port hybrid microgrid is developed. Reference [28] proposes a distributed ESS control method based on virtual inertia for AC/DC microgrid to improve system stability. A multi-time scale control method for AC/DC microgrid, which divides ESS and bidirectional power converter (BPC) into different time scales to improve the system stability under a small perturbance is described in [8].

However, these mentioned control methods can be only applied in an AC/DC hybrid microgrid with single ESS. With the increase of microgrid scale, introduction of MESS makes AC/DC hybrid microgrid improve the utilization of RESs and increase system reliability. All devices in MESS are served for storing energy, balancing power and maintaining system stability simultaneously, which brings challenges to the system control.

In this paper, a lithium battery storage system and a hydrogen energy storage system are incorporated as the multi-energy storage system for AC/DC hybrid microgrid. In this case, operating cost of each ESS and slow power response caused by the addition of HESS should be considered when designing a control method. Aiming at the studied system, a hierarchical self-regulation control is proposed to improve the power respond and achieve the economic operation.

This paper is organized as follows. Section II presents the system configuration AC/DC hybrid microgrid with hydrogen storage system. The modeling of hydrogen energy storage system and its analysis are implemented in Section III. The proposed hierarchical self-regulation control method is described in detail in Section IV. The simulation and the experimental results are subsequently provided in Section V. Lastly, conclusions are drawn in Section VI.

II. CONFIGURATION OF THE AC/DC HYBRID MICROGRID WITH MULTI-ENERGY STORAGE SYSTEM

AC/DC hybrid microgrid with hydrogen storage and battery storage is developed to explain the control strategy proposed in this paper as shown in Fig. 1, which can be observed that the studied system consists of three parts: DC subgrid, AC subgrid and AC/DC power flow controller. Both AC subgrid and DC subgrid are composed of four parts: RESs, HESS, BESS and loads. DC subgrid and AC subgrid are connected by BPC, which are responsible for power exchanging between subgrids, serving for maintaining stable operation.

The studied hybrid microgrid as shown in Fig. 1 is modeled using Simulink in MATLAB to simulate system operation and control. 25 kW PV arrays are connected to DC bus through a DC/DC boost converter. A capacitor is to suppress high frequency ripples of PV output voltage. A 20 kW wind turbine generator with doubly fed induction generator is connected to an AC bus to simulate AC sources. 200 Ah lithium batteries as one of energy storage, and 5 kW HESSs including electrolyzers, H2 tanks and fuel cells as another energy storage are connected to both DC and AC buses through DC/DC converters. Variable DC load (5 kW–20 kW) and AC load (5 kW–20 kW) are connected to DC and AC buses respectively. The rated voltages for DC and AC buses are 1000 V and 310 V rms respectively. A three phase BPC with LC filter connects DC bus to AC bus.

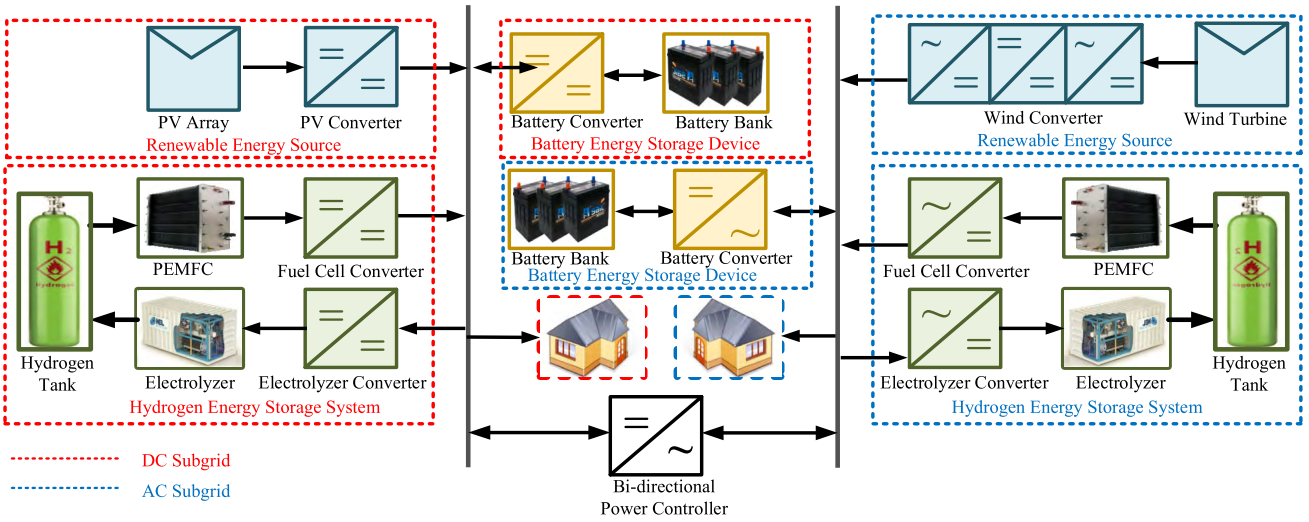

FIGURE 1. A representation of the studied system.

The basic operation rule to be satisfied of hybrid microgrid is that power produced by RESs should be preferentially used to supply load demand. Specifically, if RESs (PV and wind energy) generate greater power than load demanded, the extra power can be used to charge battery or to produce H_2 in electrolyzer. On the contrary, if RESs are unable to provide power for all loads, the insufficient power needs to be supplemented either by battery or fuel cell.

III. PROCESS MODEL OF HESS

Hydrogen is an energy carrier, which can be generated through an electrolyzer, in which water molecules are split into hydrogen and oxygen molecules. The process is referred as electrolysis, whose chemical reactions to be occurred require electricity as energy source. Subsequently, the produced hydrogen can be stored until it is further converted to meet end-use energy demands. If the end-use demand is electricity, the conversion can be executed by applying a fuel cell in which hydrogen molecules combine with oxygen to form water and electricity. Hence, the conversion of power–to–power through HESS comprises three parts:

- Hydrogen production: conversion of electrical to chemical energy in electrolyzer.
- Hydrogen storage: chemical energy storage of hydrogen in H_2 tank.
- Electricity production: conversion of chemical to electrical energy in fuel cell.

Thus, HESS is allocated to three devices, and can be regarded as a system comprised of three individual subsystems. In this section technology of these subsystems is reviewed in more detail.

A. HYDROGEN PRODUCTION: ELECTROLYZER

There are many kinds of electrolyzers, which can be differentiated by the type of electrolyte, operating temperature and charge carrier utilized. The most common types are: Alkaline electrolyzer (AEL), Proton Exchange Membrane electrolyzer (PEMEL), Solid Oxide electrolyzer (SOEL). In this paper, AELs are selected as they represent the most mature electrolyzer technology presented in the market with lower investment costs and higher efficiencies than PEMEL and SOEL.

Electrolyzer runs in current mode. Operating voltage of an electrolyzer is given as [29].

$$V_{el} = V_{rev} + \frac{r_1 + r_2 T}{A} I_{el} + s \log\left(\frac{t_1 + t_2/T + t_3/T^2}{A} I_{el} + 1\right) \quad (1)$$

where T is the operating temperature of electrolyzer, r_1 and r_2 are parameters related to internal resistance of the electrolyzer, in which r_2 reflects the change of internal resistance with temperature. s, t_1, t_2 and t_3 are related parameters of overvoltage caused by polarization of electrodes and electrolyte. t_2 and t_3 reflect the over-voltage with the change of temperature. r_1, r_2, t_1, t_2 and t_3 are all empirical parameters, which can be measured by experiments. The reversible open circuit voltage U_{rev} reflects the minimum potential between electrodes when every single electrolytic monomer is electrolyzing water. It can be obtained by (2).

$$V_{rev} = \frac{\Delta G_f}{2F} = \frac{\Delta H - T\Delta S}{2F} \quad (2)$$

where ΔG_f is changing value of Gibbs free energy. ΔH and ΔS are enthalpy and entropy changing value respectively. F is Faraday constant. Therefore, V_{rev} is calculated equaling to 1.229 V under the standard circumstance, which increases with its temperature reducing or vapor pressure increasing.

In practical application, electrolyzer is usually connected in series with several monomers to achieve the required

hydrogen. When the number of electrolytic monomers connected in series is n_{el}, the terminal voltage of the electrolyzer stack is described as follows:

$$V_{el}^{stack} = n_{el} V_{el} \tag{3}$$

B. HYDROGEN CONSUMPTION: FUEL CELL

As described previously, fuel cell is an electrochemical device in which the chemical energy stored in the form of hydrogen and oxygen is converted into electrical power. In contrast to batteries, chemical energy is not stored in the device, and hence a continuous supply of fuel and oxidant is required for the conversion process to proceed.

Fuel cell voltage is calculated based on voltage drops associated with all the losses as follows [30]:

$$V_{fc} = E_{nernst} - V_{ohm} - V_{act} - V_{con} \tag{4}$$

where E_{nernst} is open circuit voltage of fuel cell. V_{ohm}, V_{act} and V_{con} are ohm overvoltage, activated overvoltage, and concentration overvoltage respectively.

In practical application, fuel cell is usually connected in series with several monomers to form fuel cell stack. When the number of fuel cell monomers connected in series is n_{fc}, the terminal voltage of fuel cell stack is obtained as follows:

$$V_{fc}^{stack} = n_{fc} V_{fc} \tag{5}$$

C. HYDROGEN STORAGE: H_2 TANK

The capacity of HESS is determined by the quantity of gas stored in hydrogen storage tank. High-pressure hydrogen storage tank used in practice is a large volume gas tank, which can be composed of multiple gas tanks in series. Furthermore, as capacity expansion only needs to add new gas tanks, the cost of expansion is much lower than that of BESS. Hydrogen gas in hydrogen storage tank is assumed to be an ideal gas, which can be obtained by the ideal gas equation:

$$p_{tank} V_{tank} = n_{H_2} R T_{tank} \tag{6}$$

where p_{tank} is gas pressure of hydrogen tank, V_{tank} is volume of hydrogen tank, T_{tank} is temperature of gas in the hydrogen storage tank, n_{H2} is the mole number of hydrogen in hydrogen storage tanks, R is ideal gas constant, and the value is 8.3143 J/K · mol.

It can be seen that the mole number of hydrogen in hydrogen tank is directly proportional to pressure. When the upper and lower limits of available hydrogen pressure in hydrogen tank are p_{tank_max} and p_{tank_min}, max mole number of available hydrogen is described as (7).

$$n_{H_{2\_max}} = \frac{V_{tank}}{R T_{tank}} \left(p_{tank\_max} - p_{tank\_min} \right) \tag{7}$$

For this technology state of charge in hydrogen tank SOC_H is in reality a measure of gas density in the tank compared to maximum density. The density depends on the mole number of hydrogen in hydrogen tank, according to (8).

$$SOC_H\ (\%) = \frac{n_{H_2}}{n_{H_{2\_max}}} = \frac{p_{tank} - p_{tank\_min}}{p_{tank\_max} - p_{tank\_min}} \tag{8}$$

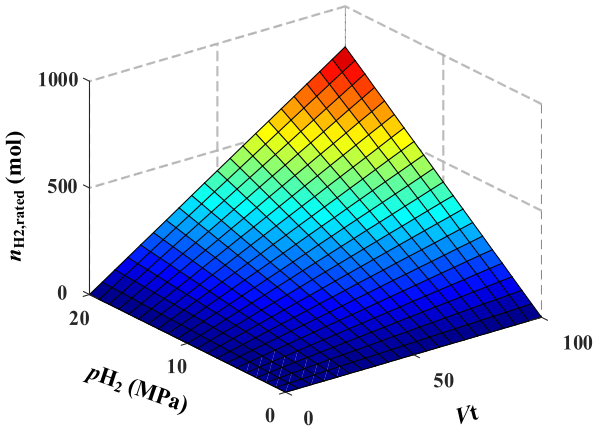

FIGURE 2. The amount of hydrogen depending on the tank volume and gas pressure.

In the operation of HESS, Fig. 2 shows relationship between hydrogen amount in the tank and gas pressure by (7).

According to type of fuel cell presented in Fig. 1, as nominal hydrogen capacity at the initial pressure of 20 Mpa is 403 mol, hydrogen consumption of fuel cells is calculated by (9).

$$n'_{H_2} = \frac{n'_{H_2,rated}}{P_{fc,rated}} \cdot P_{fc} \tag{9}$$

where n'_{H2} is hydrogen consumption by fuel cell, $n'_{H2,rated}$ is hydrogen consumption by fuel cell at the rated power and atmospheric pressure. P_{fc} and $P_{fc,rated}$ are used power and rated power of fuel cell.

The possible usage time of stored hydrogen depends on available amount of hydrogen and the consumption of hydrogen by fuel cell, which is the function from used fuel cell power, as it is presented in Fig. 3.

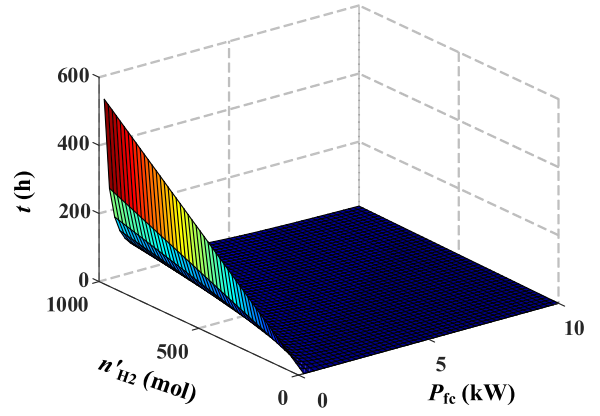

FIGURE 3. Usage time of stored hydrogen depending on the hydrogen amount and fuel cell power.

IV. CONTROL ARCHITECTURE

The proposed hierarchical self-regulation control of AC/DC hybrid microgrid with multi-energy storage systems is mainly composed of two parts, namely supervisory layer control and

local layer control. The supervisory layer control is mainly used for power distribution between HESS and BESS, while the local layer control is served for stability operation of AC/DC hybrid microgrid.

A. SUPERVISORY LAYER CONTROL

In the supervisory layer control, charging/discharging critical power is determined according to the cost of cycling energy of HESS and BESS. Fig. 4 shows supervisory layer control based on the cost of cycling energy function.

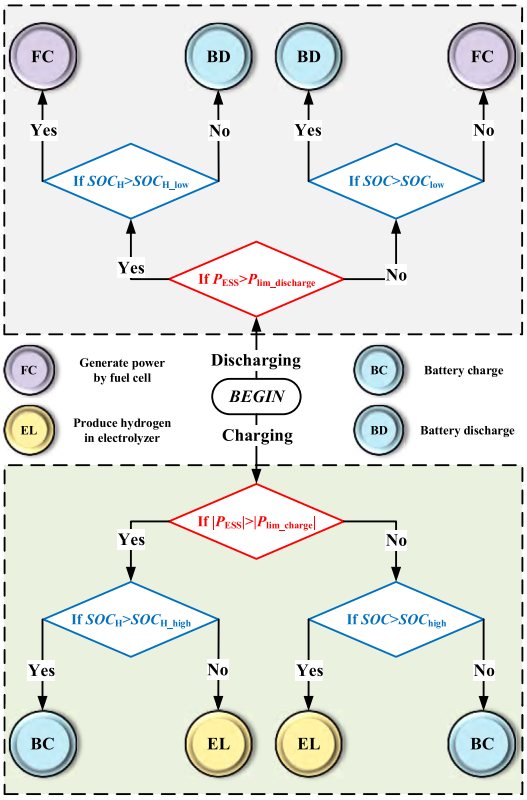

FIGURE 4. Flow chart of the proposed supervisory layer control.

It can be concluded that in the case of charging, if surplus power is less than or equal to the charging critical power, it is considered to charge battery first. When battery is charged to the upper limit of SOC, excess power is used to generate hydrogen in electrolyzer. If residual power is greater than charging critical power, it is preferred to generate hydrogen in electrolyzer. When equivalent SOC_H of hydrogen storage tank reaches the upper limit value, system will change to charge battery. In the case of discharging, when demanded power output from ESSs is less than or equal to discharging critical power, discharging from battery is preferred. When SOC of battery reaches the lower limit value, fuel cell starts to output power. If needed power is greater than discharging critical power, fuel cell outputting power is given priority. When equivalent SOC_H of hydrogen storage tank reaches the lower limit value, ESS which bear system insufficient power is selected as the battery.

1) CALCULATION OF CHARGING CRITICAL POWER

When power generated by RESs is greater than power required by loads, excess energy is used to charge battery or to generate hydrogen in electrolyzer, which subsequently is stored in hydrogen storage tank.

The cost of cycling energy corresponding to a certain power P (kW) through BESS C'_{bat} (€) including energy lost, can be calculated as:

$$C'_{bat} = \frac{P \cdot 1000 C_{bat}}{C_N N_{bat\_p} V_{DC} N_{cycles\_eq} \eta_{global\_bat}} \tag{10}$$

where C_{bat} is battery bank acquisition cost, C_N is nominal capacity of battery, N_{bat_p} is the number of batteries in parallel, V_{DC} is DC bus voltage and N_{cycles_eq} is the average of a battery lifetime in equivalent full cycles.

The cost of cycling energy of HESS is presented in (11) regardless of used power.

$$C'_{HESS} = \frac{\left(C_{EL}/\text{Life}_{EL}\right) + C_{O\ \&\ M\_EL} + \left(C_{FC}/\text{Life}_{FC}\right) + C_{O\ \&\ M\_FC}}{\eta_{EL}\eta_{FC}} \tag{11}$$

where $C_{O\&M\_EL}$ and $C_{O\&M\_FC}$ are O&M costs of electrolyzer and fuel cell, respectively.

2) CALCULATION OF DISCHARGING CRITICAL POWER

When power generated by RESs is not enough to supply loads, insufficient energy is implemented by ESSs. Discharging critical power decides the order of ESSs providing power.

The average cost of supplying power with a fuel cell depends on whether it is fed by hydrogen produced by electrolyzer, and stored in tank, or it is fed by externally purchased hydrogen. If fuel cell uses hydrogen produced previously by electrolyzer, then cost is fixed:

$$C_{FC} = \frac{C_{FC}}{\text{Life}_{FC}} + C_{O\&\ M\_FC} \tag{12}$$

Fig. 5 shows the cost of cycling energy relationship between HESS and BESS in the charging operation mode and the cost of supplying energy relationship between HESS and

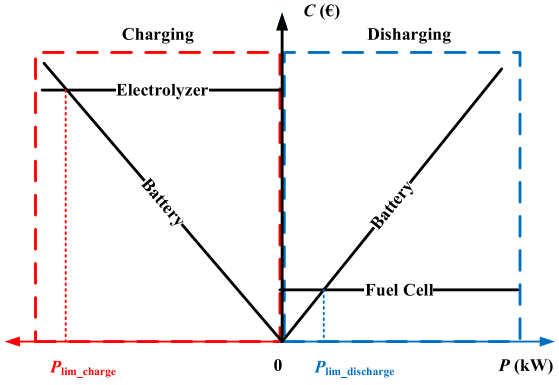

FIGURE 5. Cost relationship between the HESS and BESS in the charging operation mode and discharging operation mode.

BESS in the discharging operation mode. It can be seen that when power is less than critical power of charging $P_{\text{lim\_charge}}$, energy cost of BESS is obviously lower than HESS. In this situation, battery should be first charged. On the contrary, when power is greater than $P_{\text{lim\_charge}}$, energy cost of BESS is higher than operating cost of HESS, which enable electrolyzer produce hydrogen preferentially. When power is less than critical power of discharging $P_{\text{lim\_discharge}}$, energy cost of BESS is obviously lower than HESS. In this situation, battery should be first discharged. On the contrary, when power is greater than $P_{\text{lim\_discharge}}$, energy cost of BESS is higher than operating cost of HESS, which enable fuel cell produce electricity preferentially.

B. LOCAL LAYER CONTROL

In order to improve utilization of PV and wind energy, maximum power tracking control method is employed for renewable sources in local control layer, which has been researched a lot in [1], [12]. In this paper, that are not repeatedly described. In this section, droop control with global interactive power support is presented for energy storage devices in local control layer.

1) CONTROL OF ESSS IN AC AND DC SUBGRID

During the operation of AC/DC hybrid microgrid, when power flows from DC subgrid to AC subgrid, BPC can be regarded as a virtual synchronous generator. Similarly, when power is transferred from AC subgrid to DC subgrid, BPC can be considered as a virtual DC capacitance [29]. Thus, the following equations can be obtained:

$$\begin{cases} \dfrac{2H_{\text{VSG}}}{f_0}\dfrac{\mathrm{d}f}{\mathrm{d}t} = \Delta P_{\text{AC}} & (\text{DC} \rightarrow \text{AC}) \\ \dfrac{C_{\text{DC}}V_{\text{DC}}}{S_{\text{IC}}}\dfrac{\mathrm{d}V_{\text{DC}}}{\mathrm{d}t} = \Delta P_{\text{DC}} & (\text{AC} \rightarrow \text{DC}) \end{cases} \tag{13}$$

where H_{VSG} is inertial constant of synchronous generator, f_0 is the rated frequency of AC subgrid, C_{DC} is capacitance of DC capacitor, S_{IC} is the rated power of BPC, ΔP_{AC} and ΔP_{DC} represent the power transferred.

Based on (13), (14) can be achieved after some math operations on the premise of power balance.

$$\Delta V_{\text{DC}} = -V_{\text{REF}} + \sqrt{\frac{4H_{\text{VSG}}S_{\text{IC}}}{f_0 C_{\text{DC}}}\Delta f + V_{\text{REF}}^2} \tag{14}$$

Neglecting higher than second order, Taylor series can be employed to linearize (14), and the following equations can be obtained.

$$\begin{cases} \Delta V_{\text{DC}} = M\Delta f \\ M = \dfrac{2H_{\text{VSG}}S_{\text{IC}}}{V_{\text{REF}}C_{\text{DC}}f_0} \end{cases} \tag{15}$$

where V_{REF} is the rated voltage of DC subgrid, M is defined as the correlation coefficient between DC subgrid and AC subgrid.

Therefore, droop control with global interactive power support for energy storage devices in DC subgrid can be expressed by the following.

$$P_{\text{DC,ES}}^{\text{REF}} = \underbrace{k_{\text{DC}}\left(V_{\text{REF}} - V_{\text{DC}}\right)}_{\text{local voltage control}} \underbrace{- \left(k_{\text{DC}} + \frac{D_{\text{VSG}}}{M}\right)\Delta V_{\text{DC}}^{\text{VIR}} - \frac{2H_{\text{VSG}}}{M}\frac{\mathrm{d}\Delta V_{\text{DC}}^{\text{VIR}}}{\mathrm{d}t}}_{\text{interactive power support}} \tag{16}$$

where local voltage part is responsible for voltage regulation in DC subgrid, while interactive power support part calculated by the variation of AC frequency according to (14) is in charge of improving system stability.

Similarly, droop control with global interactive power support for energy storage devices in AC subgrid can be described by (17).

$$P_{\text{AC,ES}}^{\text{REF}} = \underbrace{k_{\text{AC}}\left(f_0 - f\right)}_{\text{local frequency control}} \underbrace{- \left(k_{\text{AC}} + D_{\text{VSG}}M\right)\Delta f^{\text{VIR}} - C_{\text{VIR}}M^2 f_0\frac{\mathrm{d}\Delta f^{\text{VIR}}}{\mathrm{d}t}}_{\text{interactive power support}} \tag{17}$$

where local frequency part is responsible for frequency regulation in AC subgrid, while interactive power support part calculated by the variation of DC voltage according to (14) is in charge of improving power response.

Fig. 6 shows control scheme of the proposed method, which can be divided into two parts: each ESS controller obtains reference power value provided or absorbed according to local layer control method with global power support, and then selects the most economical ESS type from supervisory layer control method according to the obtained reference power value. In Fig. 6, dotted line part is the proposed control strategy scheme and solid line part is the normal power controller structure.

2) CONTROL OF BPC

BPC is used to control the power transfer between AC and DC subgrids. In order to enhance inertia of the whole system, especially the inertia of the DC subgrid, the virtual inertia equation as shown in the following equation is added to the voltage outer loop.

$$I_{\text{REF}} - I_{\text{o}} - D_{\text{b}}(V_{\text{dc}}^* - V_{\text{n}}) = C_{\text{v}}V_{\text{n}}\frac{\mathrm{d}V_{\text{dc}}^*}{\mathrm{d}t} \tag{18}$$

where I_{REF} and I_{o} are reference output current and actual output current of DC converters, D_{b} is V/I droop coefficients, C_{v} is capacity of virtual capacitor.

According to the BPC control shown in Fig. 6, small signal model of current inner loop can be expressed as:

$$\begin{cases} \Delta I_{\text{d}}(s) = \left[\Delta I_{\text{d}}^*(s) - \Delta I_{\text{d}}(s)\right]G_i(s)\big/(Ls + r) \\ \Delta I_{\text{q}}(s) = \left[\Delta I_{\text{q}}^*(s) - \Delta I_{\text{q}}(s)\right]G_i(s)\big/(Ls + r) \end{cases} \tag{19}$$

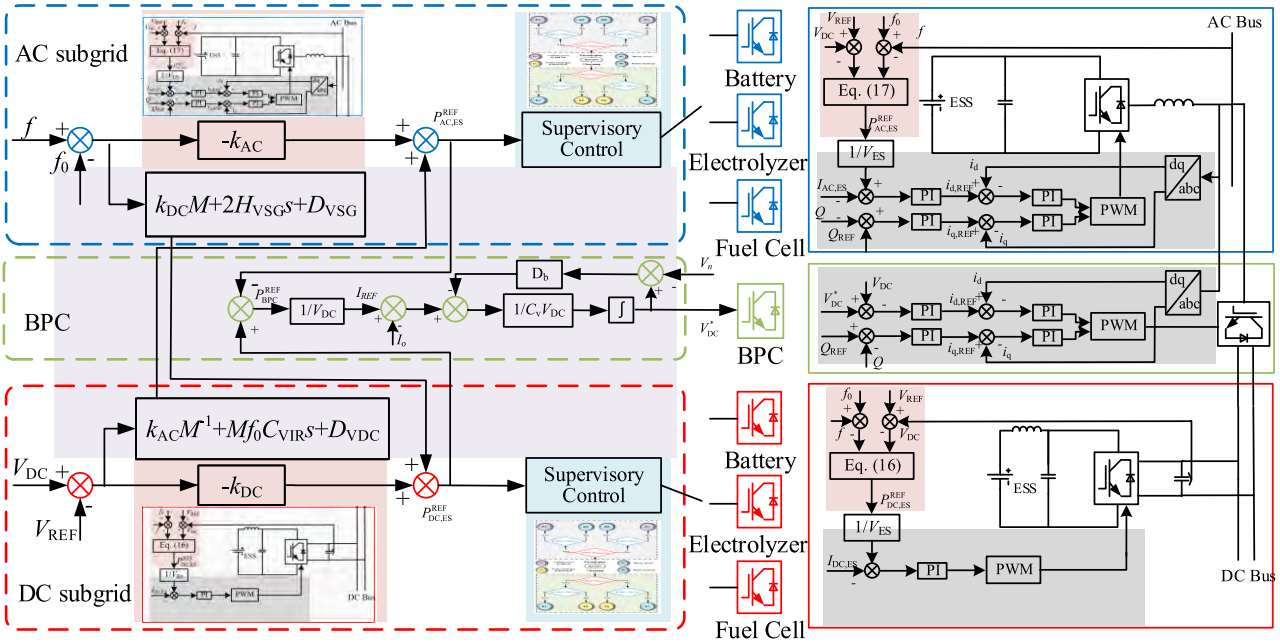

FIGURE 6. Control scheme of the proposed strategy.

Under the condition that only active power is considered, voltage outer loop can be expressed as:

$$\frac{3}{2}\left(V_{\mathrm{d}}\Delta I_{\mathrm{d}}+\Delta V_{\mathrm{d}}I_{\mathrm{d}}\right)=CV_{\mathrm{dc}}\frac{\mathrm{d}\Delta V_{\mathrm{dc}}}{\mathrm{d}t}+V_{\mathrm{dc}}\Delta I_{\mathrm{o}}+\Delta V_{\mathrm{dc}}I_{\mathrm{o}} \tag{20}$$

where r is equivalent series resistance of inductance L, i_{d} and I_{q} are respectively d and q components BPC output current in dq coordinate system. V_{d} and V_{q} are respectively d and q components BPC output voltage in dq coordinate system.

The relationship between $\Delta V_{\mathrm{dc}}(\mathrm{s})$ and $\Delta I_{\mathrm{d}}(\mathrm{s})$, $\Delta V_{\mathrm{dc}}(\mathrm{s})$ and $\Delta I_{\mathrm{o}}(\mathrm{s})$, $\Delta V_{\mathrm{dc}}(\mathrm{s})$ and $\Delta V_{\mathrm{d}}(\mathrm{s})$ can be obtained respectively by using superposition theorem.

$$\frac{\Delta V_{\mathrm{dc}}(s)}{\Delta I_{\mathrm{d}}(s)}=\frac{3V_{\mathrm{d}}}{2\left(CV_{\mathrm{dc}}s+I_{\mathrm{o}}\right)} \tag{21}$$

$$\frac{\Delta V_{\mathrm{dc}}(s)}{\Delta I_{\mathrm{o}}(s)}=\frac{V_{\mathrm{d}}}{CV_{\mathrm{dc}}s+I_{\mathrm{o}}} \tag{22}$$

$$\frac{\Delta V_{\mathrm{dc}}(s)}{\Delta V_{\mathrm{q}}(s)}=\frac{3I_{\mathrm{q}}}{2\left(CV_{\mathrm{dc}}s+I_{\mathrm{o}}\right)} \tag{23}$$

Small signal decomposition is carried out on the virtual inertia equation shown in (18), and the following small signal model can be obtained:

$$\Delta V_{\mathrm{dc}}^{*}(s)=\left(-\Delta I_{\mathrm{o}}(s)-D_{\mathrm{b}}\Delta V_{\mathrm{dc}}^{*}(s)\right)\frac{1}{C_{\mathrm{v}}V_{\mathrm{n}}}\frac{1}{s} \tag{24}$$

Therefore, the closed-loop transfer function of BPC control between $\Delta V_{\mathrm{dc}}(\mathrm{s})$ and $-\Delta I_{\mathrm{o}}(\mathrm{s})$ can be obtained as follows:

$$G(s)=\frac{b_0s^2+b_1s+b_2}{a_0s^5+a_1s^4+a_2s^3+a_3s^2+a_4s+a_5} \tag{25}$$

$$\begin{cases}a_0=2CLV_{\mathrm{dc}}C_{\mathrm{v}}V_{\mathrm{n}}\\ a_1=2C_{\mathrm{v}}V_{\mathrm{n}}\left(Ck_{\mathrm{pi}}K_{\mathrm{pwm}}V_{\mathrm{dc}}+I_{\mathrm{o}}L\right)+2CLD_{\mathrm{b}}V_{\mathrm{dc}}\\ a_2=C_{\mathrm{v}}K_{\mathrm{pwm}}V_{\mathrm{n}}\left(2Ck_{\mathrm{ii}}V_{\mathrm{dc}}+3k_{\mathrm{pi}}k_{\mathrm{pv}}V_{\mathrm{d}}+2I_{\mathrm{o}}k_{\mathrm{pi}}\right)\\ \quad +2D_{\mathrm{b}}\left(Ck_{\mathrm{pi}}K_{\mathrm{pwm}}V_{\mathrm{dc}}+I_{\mathrm{o}}L\right)\\ a_3=C_{\mathrm{v}}K_{\mathrm{pwm}}V_{\mathrm{n}}\left(3k_{\mathrm{ii}}k_{\mathrm{pv}}V_{\mathrm{d}}+3k_{\mathrm{iv}}k_{\mathrm{pi}}V_{\mathrm{d}}+2I_{\mathrm{o}}k_{\mathrm{ii}}\right)\\ \quad +D_{\mathrm{b}}K_{\mathrm{pwm}}\left(2Ck_{\mathrm{ii}}V_{\mathrm{dc}}+3k_{\mathrm{pi}}k_{\mathrm{pv}}V_{\mathrm{d}}+2I_{\mathrm{o}}k_{\mathrm{pi}}\right)\\ a_4=D_{\mathrm{b}}K_{\mathrm{pwm}}\left(3k_{\mathrm{ii}}k_{\mathrm{pv}}V_{\mathrm{d}}+3k_{\mathrm{iv}}k_{\mathrm{pi}}V_{\mathrm{d}}+2I_{\mathrm{o}}k_{\mathrm{ii}}\right)\\ \quad +3k_{\mathrm{ii}}k_{\mathrm{iv}}K_{\mathrm{pwm}}V_{\mathrm{d}}C_{\mathrm{v}}V_{\mathrm{n}}\\ a_5=3k_{\mathrm{ii}}k_{\mathrm{iv}}K_{\mathrm{pwm}}V_{\mathrm{d}}D_{\mathrm{b}}\end{cases}$$

$$\begin{cases}b_0=3k_{\mathrm{pi}}k_{\mathrm{pv}}K_{\mathrm{pwm}}V_{\mathrm{d}}\\ b_1=3k_{\mathrm{ii}}k_{\mathrm{pv}}K_{\mathrm{pwm}}V_{\mathrm{d}}+3k_{\mathrm{iv}}k_{\mathrm{pi}}K_{\mathrm{pwm}}V_{\mathrm{d}}\\ b_2=3k_{\mathrm{ii}}k_{\mathrm{iv}}K_{\mathrm{pwm}}V_{\mathrm{d}}\end{cases}$$

Due to the physical meaning of step response indicating that DC bus voltage variation ΔV_{dc} response over time, when output current of BPC reduce 1 A, the step response of $G(\mathrm{s})$ is introduce to analyze relationship of different parameters. Fig. 7 and Fig. 8 respectively show the condition of different C_{v} and $D_{\mathrm{b}}=1$, $D_{\mathrm{b}}=5$.

It can be seen that after virtual inertial control is added into the control of BPC, bus voltage step response rises smoothly to a stable value, and the dynamic change process of DC bus voltage is improved. Furthermore, the larger C_{v} is, the more gentle change of DC bus voltage is, which indicates system owes greater inertia simultaneously. When $C_{\mathrm{v}}<30\ \mu$F,

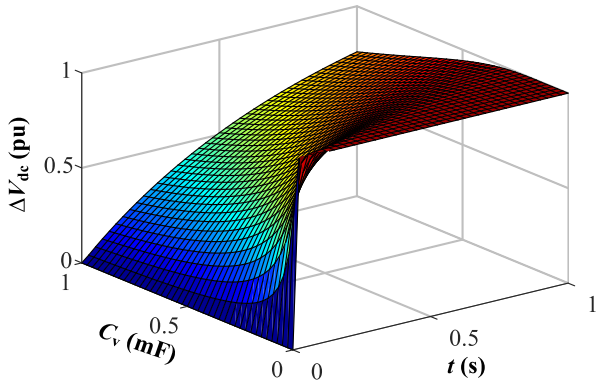

FIGURE 7. Unit-step responses of G (s) with $D_b = 1$.

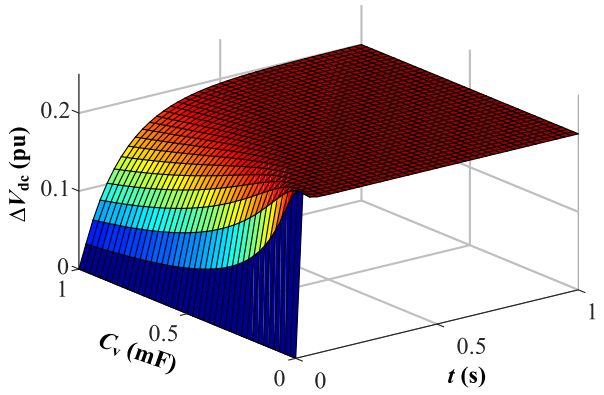

FIGURE 8. Unit-step responses of G(s) with $D_b = 5$.

DC bus voltage change fast, which shows very small inertia of system. So it can be concluded that the value of C_v directly decide system inertia.

As can be seen from Fig. 9, the smaller D_b is, the longer time DC bus voltage spends to stabilize, which means greater virtual inertia of the whole system. Otherwise, the larger D_b is, the shorter time is when DC bus voltage tends to be stable, which leads to the smaller virtual inertia. Since both C_v and D_b can affect system virtual inertia, selection of D_b value should consider the influence of droop control.

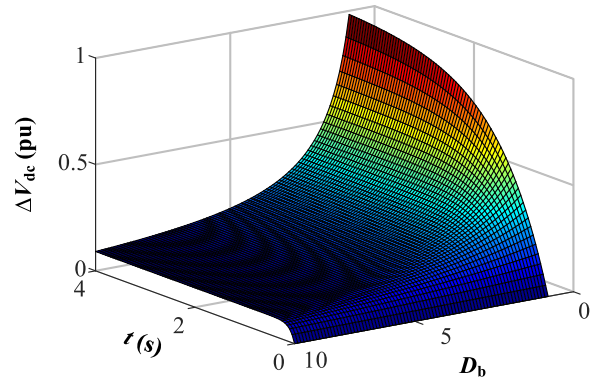

FIGURE 9. Unit-step responses of G (s) with different D_b.

V. RESULTS AND DISCUSSION

In order to validate the proposed hierarchical self-regulation control method, a AC/DC hybrid microgrid with multi-energy storage systems is developed based on Fig. 1 in RT-LAB simulation platform, as shown in Fig. 10. RT-LAB simulation platform transmits simulation model from host computer to target computer. The generated codes of Matlab/Simulink model and monitored data are transferred between host computer and target machine based on TCP/IP communication.

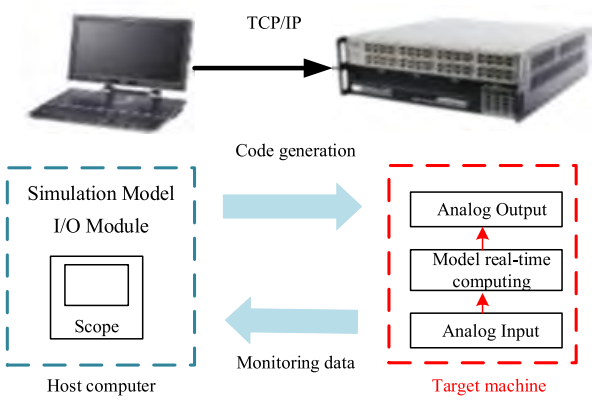

FIGURE 10. Configuration of RT-LAB simulation platform.

In the studied system, ESS contains battery and fuel cell during discharging process, while battery and electrolyzer during charging operation. All RESs in the studied system are operating with maximum power point tracking method. So that the dynamic performance are just influenced by response of ESSs and BPC. Controller parameters in AC subgrid, DC subgrid and BPC part are respectively shown in TABLE 1. Economic parameters of battery, fuel cell and electrolyzer are respectively shown in TABLE 2.

TABLE 1. System control parameters.

Unit	Parameters	Value
AC Subgrid	Nominal frequency: f/Hz	50
	Droop coefficent: k_{AC}/(MW/Hz)	17.3
	Virtual inertia constant: H_{VSG}/s	$6.5*10^{-3}$
	Virtual damping coefficent: D_{VSG}	20
	Rated power of DES unit/kW	30
	Nominal voltage: V_{REF}/kV	1
DC Subgrid	Droop coefficent: k_{DC}/(MW/ kV)	15.8
	DC capacitor: C_{DC}/mF	7.5
	Virtual damping coefficent: D_{VDC}	20
	Rated power of DES unit/kW	30
BPC	Rated power:S_{IC}/kVA	20
	V/I droop coefficients: D_b	4.5
	Capacity of virtual capacitor: C_v	20

A. A 24 H OPERATION SIMULATION

A 24 hours operation of AC/DC hybrid microgrid with hydrogen energy storage system using both proposed control

TABLE 2. Operation cost parameters.

Unit	Parameters	Value
Fuel cell	Acquisition cost: C_{FC}/€	4000
	O&M cost: $C_{O\&M\_FC}$/€/h	0.2
	Expected lifetime: $Life_{FC}$/ h	30,000
	Corresponding to 50% of the H_2 lower heating value:η_{FC}/ kWh/ kgH_2	16.66
	Rated power/kW	5
Electrolyzer	Acquisition cost: C_{EL}/€	3200
	O&M cost: $C_{O\&M\_EL}$ /€/h	0.2
	Expected lifetime: $Life_{EL}$/ h	30,000
	Corresponding to 85% of the higher heating value of H_2: η_{EL}/ kgH_2/kWh	0.021517
	Rated power/kW	5
Battery	Acquisition cost: C_{bat}/€	22,600
	Overall efficiency of the batteries: $\eta_{global\ bat}$	0.6
	Average of a battery lifetime in equivalent full cycles: $N_{cycles\ eq}$	4,000
	Rated power/kW	5

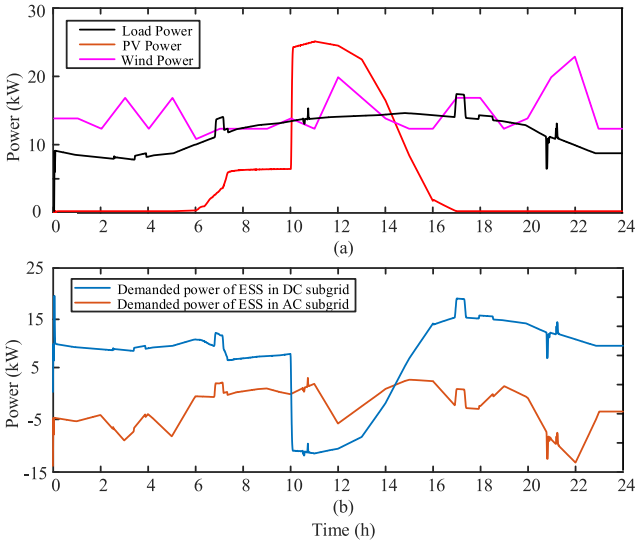

FIGURE 11. Basic operation condition. (a) RES power generation and load power. (b) Demanded power of ESS in DC and AC subgrid.

method and only droop control method. Fig.11 shows basic operation condition during 24 hours, where RESs generation power and load power are shown in Fig. 11(a).

The highest power of PV power generation system connected to DC subgrid is about 25 kW at 11:00 during the day. While wind power generation system connected to AC subgrid has a maximum power of about 21 kW at 22:00. Fig.11(b) shows the power to be supplied or absorbed by ESS in AC and DC subgrids, respectively. Line in blue represents power required of ESS in DC subgrid and line in orange represents power required of ESS in AC subgrid.

In order to analyze the performance of proposed hierarchical self-regulation control method, only droop control which has been researched a lot previously is adopted. Simulation results of these two methods are respectively

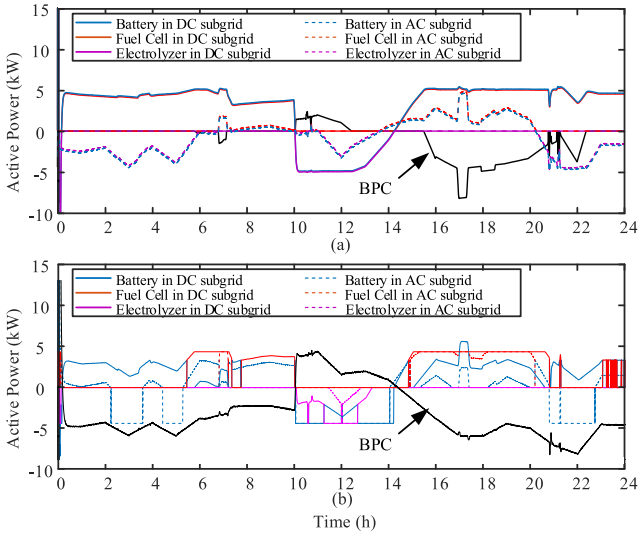

FIGURE 12. Output power of ESS in AC and DC subgrid under different control methods. (a) Only droop control method. (b) Proposed control method.

shown in Fig. 12(a) and Fig. 12(b). Wave forms include ESSs output in AC and DC subgrid and exchanging power of BPC, where dotted line represents AC subgrid and solid line stands for DC subgrid.

As shown in Fig. 12(a), when only droop control method is utilized, output or absorption power of each energy storage device of ESS will be equally distributed. Specifically, when power vacancy appears in system, ESS works in discharging mode. That is power averagely supplied by battery and fuel cell due to the equal droop coefficient. Similarly when surplus power occurs in system, ESS operates in charging mode. Electrolyzer and battery absorb surplus power equally.

As shown in Fig. 12(b), when proposed hierarchical self-regulation control method is adopted, output or absorption power of each energy storage device of ESSs will be allocated according to supervisory layer control described in Section IV. In charging mode, when demand power of ESSs is in the range of [0,5000], sufficient power is absorbed by batteries. When demand power of ESSs is in the range of [5000,7360], abundant power is first balanced by battery, and unabsorbable power of battery is transferred to electrolyzers. On the contrary, when demand power of ESSs is in the range of [7360, 10000], surplus power is first balanced by electrolyzers, and batteries are charged by remaining power.

In the case of discharging operation, when ESS output power is in the range of [0,3832], battery discharge to balance system power. When ESS output power is in the range of [3832,5000], fuel cell produces power to supply load. When ESS output power is in the range of [5000,10000], fuel cell produces maximum power of 5 kW, and remaining vacancy power is balanced by battery.

In order to show the control effect of AC/DC hybrid microgrid clearly under different control methods, indexes of measuring system stability are shown in Fig. 13. Frequency of AC subgrid is presented in Fig. 13(a) and Fig. 13(b) shows voltage of DC bus.

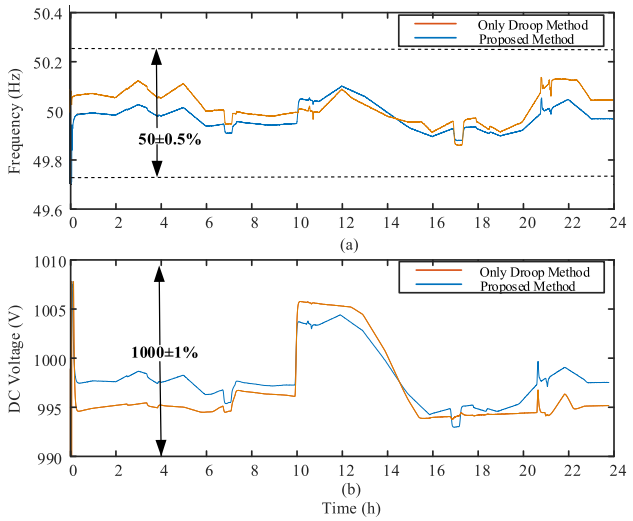

FIGURE 13. AC frequency and DC voltage under different control methods. (a) Only droop control method. (b) Proposed control method.

As shown in Fig. 13(a), compared with the proposed control method, AC frequency fluctuation under only droop control method is greater. During 0:00-10:00 and 14:00-24:00, AC frequency of proposed control method is closer to the reference value of 50 Hz than that of only droop control method. Between 10:00 and 14:00, although AC frequency fluctuation range of the proposed control method is larger than that of only droop control method, maximum difference between these two methods is not significant. Therefore, in general, the proposed control method effectively reduces fluctuation range of AC frequency during the operation of AC/DC hybrid microgrid.

For the fluctuation of DC bus voltage as shown in Fig. 13(b), it can be seen that fluctuation of DC bus voltage under these two control methods are both small, about ±0.8%. Generally speaking, DC bus voltage using proposed control method is closer to the rated value of 1000V than only droop control method. Therefore, it can be concluded that the proposed control method can also effectively improve fluctuation of DC bus voltage.

In order to express fluctuation of AC frequency and DC bus voltage more intuitively, frequency and voltage difference under these two control methods are presented in TABLE 3.

TABLE 3. Difference of voltage and frequency.

	Only droop control method			Proposed control method		
	Mean value	Maximum	Minimum	Mean value	Maximum	Minimum
V_{dc}	4.5992	7.6871	-5.8139	2.6963	6.7114	-2.4497
f	0.0371	0.0984	-0.0923	0.0305	0.0741	-0.0787

Under the only droop control method, maximum difference between DC bus voltage and rated value is about 7.6871 V and the minimum is 5.8139 V, which are 0.9757 and 3.3642 larger than the maximum difference and minimum difference under proposed control method respectively. It can also be seen from the difference of frequency in TABLE 3 that the difference between AC frequency and rated value under proposed control method is superior to only droop control method in terms of both average value and maximum/minimum value.

Fig. 14 shows the cumulative cost of ESS in DC and AC subgrids during one day operation under different control methods. Blue denotes DC subgrid and red denotes AC subgrid. Solid line represents only droop control method and dotted line represents proposed control method.

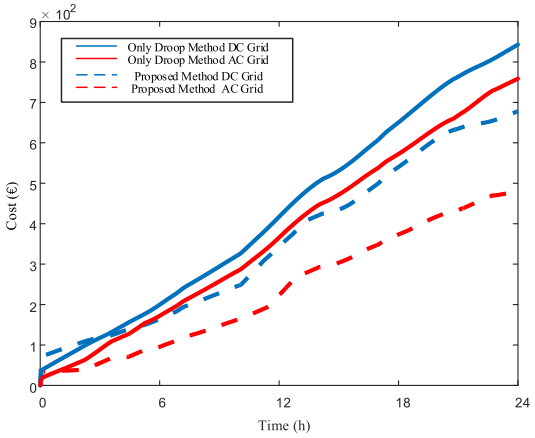

FIGURE 14. Cumulative cost of ESS in DC and AC subgrids under different control methods.

It can be seen from Fig. 14 that ESS cost of DC and AC parts under proposed method is less than that of only droop control method. Simultaneously, TABLE 4 shows the cost of ESS both in DC/AC subgrid and whole AC/DC hybrid microgrid in one day under different control methods. Compared with only droop control method, ESS cost of the proposed control method in DC subgrid, AC subgrid and the whole system respectively reduce 19.05%, 36.77% and 27.71%.

TABLE 4. Cost under different control methods.

Control methods	AC Grid/€	DC Grid/€	Total/€
Only droop control method	758.82	843.09	1601.9
Proposed control method.	479.74	678.28	1158

B. STEP POWER CHANGE

In order to show the effectiveness of proposed control method in improving virtual inertia more clearly, this section discusses examples of step power change.

Fig. 15 shows AC load decreases from 18 kW to 8 kw at the time of 4 s. At 14 s, system recovers to the initial state. Simulation results of only droop control method and proposed control method are presented. When only droop control method is adopted, ESS in AC subgrid will absorb surplus power in priority. While under the proposed control,

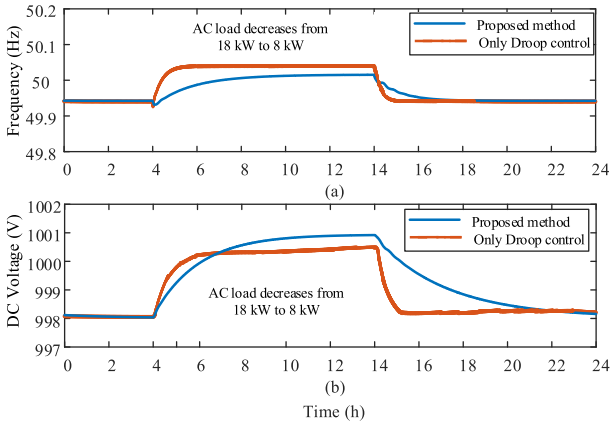

FIGURE 15. Results of frequency and DC voltage when AC load decreases.

sufficient power allocated of ESS both in AC subgrid and DC subgrid.

Fig. 15(a) shows AC frequency and Fig. 15(b) indicates DC bus voltage. Because of the more input power in DC subgrids, DC voltage increases larger and AC frequency increase smaller when using proposed method. However, it can still be concluded that proposed control method has improved system inertia.

Similar with the condition of step power change in AC subrid, simulation results of only droop control method and proposed control method are shown in Fig. 16. The system operates stably in the above operating condition, while at the time of 4s, PV output power in DC subgrid decreases from 20 kW to 10 kw. At 14 s, system recovers to the initial state.

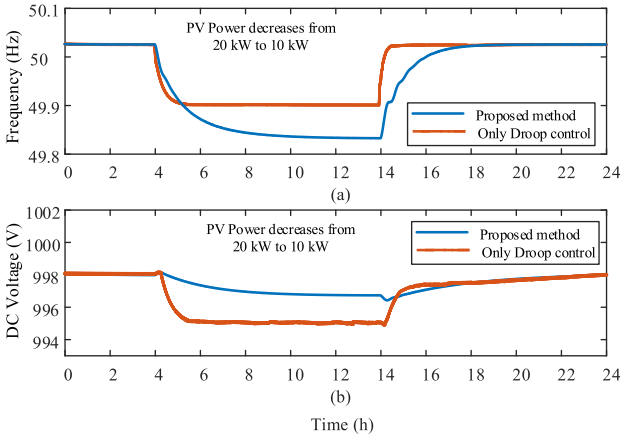

FIGURE 16. Results of frequency and DC voltage when PV output power decreases.

Fig. 16(a) shows AC frequency and Fig. 16(b) indicates DC bus voltage. Because of the more output power in AC subgrids, AC frequency drops larger and DC voltage drops smaller when using proposed method. However, it can still be seen clearly that proposed control method can enhance inertia of whole system and improve system stability.

In these two cases, we can draw a conclusion that when step power change occurs in AC subgrid, AC frequency fluctuation range controlled by proposed control method is smaller than that of only droop control method, but the fluctuation range of DC bus voltage is larger than that of droop control. Similarly, when step power change appears in DC subgrid, fluctuation range of DC bus voltage under proposed control method is smaller than that of only droop control method, but fluctuation range of AC frequency is larger than that of only droop control method. At the same time, it is also worth noting that AC frequency and DC bus voltage change more slowly when power change happens, which means that system inertia has been improved.

VI. CONCLUSION

In this paper, a hierarchical self-regulation control method is proposed for AC/DC hybrid microgrid with MESS. The supervisory layer control of this proposed control method based on operation cost of different energy storage devices, aims at minimizing ESSs operation cost. It is used to realize power economic distribution of ESSs between AC and DC subgrid and achieve economic optimum of system. The local layer control adopts virtual inertial control method with global power support, which can enhance system stability and improve system inertia. In order to validate the proposed control method, an AC/DC hybrid microgrid with MESS containing HESS and BESS is developed in Matlab/Simulink. Simulation results of AC/DC hybrid microgrid with MESS in one day show that compared with only droop control method, the proposed control method can reduce operation cost of whole system by 27.71%, and at the same time reduce DC bus voltage fluctuation of 1.9029V and AC frequency fluctuation of 0.0066Hz on average. Results of step power change show that proposed control method can also slow down changing speed of frequency and voltage and improve system inertia when power changes.

REFERENCES

[1] D. Zhou, A. Al-Durra, K. Zhang, A. Ravey, and F. Gao, "A robust prognostic indicator for renewable energy technologies: A novel error correction grey prediction model," *IEEE Trans. Ind. Electron.*, to be published.
[2] C. Wang, L. Guo, and P. Li, "Optimal dispatch and design of microgrid system," in *Handbook of Clean Energy Systems*. Hoboken, NJ, USA: Wiley, 2015, pp. 1–18.
[3] L. Guo, W. Liu, X. Li, Y. Liu, B. Jiao, W. Wang, C. Wang, and F. Li, "Energy management system for stand-alone wind-powered-desalination microgrid," *IEEE Trans. Smart Grid*, vol. 7, no. 2, pp. 1079–1087, Mar. 2016.
[4] W. Dong, Q. Yang, and X. Fang, "Multi-step ahead wind power generation prediction based on hybrid machine learning techniques," *Energies*, vol. 11, no. 8, p. 1975, 2018.
[5] H. Jia, Y. Mu, and Y. Qi, "A statistical model to determine the capacity of battery–supercapacitor hybrid energy storage system in autonomous microgrid," *Int. J. Elect. Power Energy Syst.*, vol. 54, pp. 516–524, Jan. 2014.
[6] X. Liu, P. Wang, and P. C. Loh, "A hybrid AC/DC microgrid and its coordination control," *IEEE Trans. Smart Grid*, vol. 2, no. 2, pp. 278–286, Jun. 2011.
[7] C. Wang, X. Li, L. Guo, and Y. W. Li, "A nonlinear-disturbance-observer-based DC-bus voltage control for a hybrid AC/DC microgrid," *IEEE Trans. Power Electron.*, vol. 29, no. 11, pp. 6162–6177, Nov. 2014.
[8] Y. Xia, W. Wei, M. Yu, Y. Peng, and J. Tang, "Decentralized multi-time scale power control for a hybrid AC/DC microgrid with multiple subgrids," *IEEE Trans. Power Electron.*, vol. 33, no. 5, pp. 4061–4072, May 2017.
[9] H. Qiu, B. Zhao, W. Gu, and R. Bo, "Bi-level two-stage robust optimal scheduling for AC/DC hybrid multi-microgrids," *IEEE Trans. Smart Grid*, vol. 9, no. 5, pp. 5455–5466, Sep. 2018.

[10] H. Zeng, H. Zhao, and Q. Yang, "Coordinated energy management in autonomous hybrid AC/DC microgrids," in *Proc. Int. Conf. Power Syst. Technol.*, 2014, pp. 3186–3193.
[11] N. Liu, L. He, X. Yu, and L. Ma, "Multiparty energy management for grid-connected microgrids with heat- and electricity-coupled demand response," *IEEE Trans. Ind. Informat.*, vol. 14, no. 5, pp. 1887–1897, May 2018.
[12] X. Jin, Y. Mu, H. Jia, J. Wu, T. Jiang, and X. Yu, "Dynamic economic dispatch of a hybrid energy microgrid considering building based virtual energy storage system," *Appl. Energy*, vol. 194, pp. 386–398, May 2017.
[13] Y. Xu, J. Hu, W. Gu, W. Su, and W. Liu, "Real-time distributed control of battery energy storage systems for security constrained DC-OPF," *IEEE Trans. Smart Grid*, vol. 9, no. 3, pp. 1580–1589, May 2016.
[14] Y. Gao, F. Xue, W. Yang, Q. Yang, Y. Sun, Y. Sun, H. Liang, and P. Li, "Optimal operation modes of photovoltaic-battery energy storage system based power plants considering typical scenarios," *Protection Control Mod. Power Syst.*, vol. 2, no. 1, p. 36, 2017.
[15] J. Li, J. Lin, Y. Song, X. Xing, and C. Fu, "Operation optimization of power to hydrogen and heat (P2HH) in ADN coordinated with the district heating network," *IEEE Trans. Sustain. Energy*, to be published.
[16] L. Guo, Z. Yu, C. Wang, F. Li, J. Schiettekatte, J.-C. Deslauriers, and L. Bai, "Optimal design of battery energy storage system for a wind–diesel off-grid power system in a remote Canadian community," *IET Gener., Transmiss. Distrib.*, vol. 10, no. 3, pp. 608–616, 2016.
[17] H. Yang, S. Li, Q. Li, and W. Chen, "Hierarchical distributed control for decentralized battery energy storage system based on consensus algorithm with pinning node," *Protection Control Mod. Power Syst.*, vol. 3, no. 1, p. 6, 2018.
[18] S. You, J. Hu, Y. Zong, and J. Lin, "Value assessment of hydrogen-based electrical energy storage in view of electricity spot market," *J. Mod. Power Syst. Clean Energy*, vol. 4, no. 4, pp. 626–635, 2016.
[19] J. Liu, W. Luo, X. Yang, and L. Wu, "Robust model-based fault diagnosis for PEM fuel cell air-feed system," *IEEE Trans. Ind. Electron.*, vol. 63, no. 5, pp. 3261–3270, May 2016.
[20] Q. Li, W. Chen, Z. Liu, M. Li, and L. Ma, "Development of energy management system based on a power sharing strategy for a fuel cell-battery-supercapacitor hybrid tramway," *J. Power Sources*, vol. 279, pp. 267–280, Apr. 2015.
[21] G. Cau, D. Cocco, M. Petrollese, S. K. Kær, and C. Milan, "Energy management strategy based on short-term generation scheduling for a renewable microgrid using a hydrogen storage system," *Energy Convers. Manage.*, vol. 87, pp. 820–831, Nov. 2014.
[22] F. Díaz-González, A. Sumper, O. Gomis-Bellmunt, and R. Villafáfila-Robles, "A review of energy storage technologies for wind power applications," *Renew. Sustain. Energy Rev.*, vol. 16, no. 4, pp. 2154–2171, May 2012.
[23] Q. Li, T. Wang, C. Dai, W. Chen, and L. Ma, "Power management strategy based on adaptive droop control for a fuel cell-battery-supercapacitor hybrid tramway," *IEEE Trans. Veh. Technol.*, vol. 67, no. 7, pp. 5658–5670, Jul. 2017.
[24] P. C. Loh, D. Li, Y. K. Chai, and F. Blaabjerg, "Autonomous control of interlinking converter with energy storage in hybrid AC-DC microgrid," *IEEE Trans. Ind. Appl.*, vol. 49, no. 3, pp. 1374–1382, May/Jun. 2013.
[25] P. Wang, C. Jin, D. Zhu, Y. Tang, P. C. Loh, and F. H. Choo, "Distributed control for autonomous operation of a three-port AC/DC/DS hybrid microgrid," *IEEE Trans. Ind. Electron.*, vol. 62, no. 2, pp. 1279–1290, Feb. 2015.
[26] H. Yang, Y. Qiu, Q. Li, and W. Chen, "A self-convergence droop control of no communication based on double-quadrant state of charge in DC microgrid applications," *J. Renew. Sustain. Energy*, vol. 9, no. 3, 2017, Art. no. 034102.
[27] X. Yang, H. Hu, Y. Ge, S. Aatif, Z. He, and S. Gao, "An improved droop control strategy for VSC-based MVDC traction power supply system," *IEEE Trans. Ind. Appl.*, vol. 54, no. 5, pp. 5173–5186, Sep./Oct. 2018.
[28] L. He, Y. Li, Z. Shuai, J. M. Guerrero, Y. Cao, M. Wen, W. Wang, and J. Shi, "A flexible power control strategy for hybrid AC/DC zones of shipboard power system with distributed energy storages," *IEEE Trans. Ind. Informat.*, vol. 14, no. 12, pp. 5496–5508, Dec. 2018.
[29] Ø. Ulleberg, "Modeling of advanced alkaline electrolyzers: A system simulation approach," *Int. J. Hydrogen Energy*, vol. 28, no. 1, pp. 21–33, 2003.
[30] R. F. Mann, J. C. Amphlett, M. A. I. Hooper, H. M. Jensen, B. A. Peppley, and P. R. Roberge, "Development and application of a generalised steady-state electrochemical model for a PEM fuel cell," *J. Power Sources*, vol. 86, nos. 1–2, pp. 173–180, 2000.

HANQING YANG (S'19) received the B.E. degree from the School of Electrical Engineering and Automation, Southwest Jiaotong University, Chengdu, China, in 2014, where she is currently pursuing the Ph.D. degree with the School of Electrical Engineering. Her current research interests include the areas of operation control of microgrid and optimization of distributed generation systems.

QI LI (M'12–SM'15) received the B.S. and Ph.D. degrees from the Electrical Engineering School, Southwest Jiaotong University, Chengdu, China, in 2002 and 2011, respectively. He did research as a Visiting Scholar at the School of Electrical and Electronic Engineering, Nanyang Technological University, Singapore, from 2009 to 2011. He is currently a Full Professor with the Electrical Engineering School, Southwest Jiaotong University. His research interests include optimal control of fuel cell locomotives, energy management of hybrid power systems, and optimization and control of integrated energy systems. He is a Fellow of IET. In 2019, he is nominated as the Sub-Committee Chair of the Technical Committee on Transportation Electrification of the IEEE Industrial Electronics Society. He is also an Associate Editor of Industrial Electronics Technology News of the IEEE Industrial Electronics Society.

SHUDAN ZHAO received the B.E. degree from the Electrical Engineering School, Southwest Jiaotong University, Chengdu, China, in 2018, where she is currently pursuing the master's degree. Her current research interest includes operation control of microgrid.

WEIRONG CHEN (M'99–SM'16) received the B.S. and M.S. degrees in electronic engineering from Electronic Science and Technology University, in 1985 and 1988, respectively, and the Ph.D. degree in power system and its automation from Southwest Jiaotong University, Chengdu, China, in 1998.

He was a Senior Visiting Scholar with Brunel University, England, in 1999. He is currently a Professor with the School of Electrical Engineering, Southwest Jiaotong University. He has published more than 120 refereed journals and conference papers and six books, and holds more than 40 Chinese patents. His research interests include renewable energy and its applications, fuel cell locomotive technology, and power system control. He is a Fellow of IET. He received the William F. Meggers Award and the Adolph Lomb Medal (OSA).

HONG LIU received the master's degree in energy system analysis from Tsinghua University, Beijing, China, in 1992, and the Ph.D. degree in architecture technical science from Tianjin University, Tianjin, China, in 2006. She is currently a Research Professor with the Energy Research Institute, National Development and Reform Commission, China. Her research interests include strategic and policy study on energy system optimization, energy efficiency, and comprehensive energy management.